Enhancing the performance of Alumina-pillared clay for Phenol removal from water solutions and Polyphenol removal from Olive Mill Wastewater: Characterization, kinetics, adsorption performance, and mechanism

Soukaina El Abbadi [a], Hajar El Moustansiri [a], Mohamed Douma [a, *], Abdelmjid Bouazizi [a, b, *], Brahim Arfoy [c], José Ignacio Calvo [d, e], Najib Tijani [a]

[a] *Materials, Membranes and Nanotechnology Laboratory, Moulay Ismail University of Meknès, Faculty of Sciences, BP: 11201 Zitoune Meknès, Morocco*

[b] *Department of Sciences, Ecole Normal Superieure, Moulay Ismail University of Meknès, 50000 Morocco*

[c] *Solid-State Chemistry Laboratory, Abdelmalek Essaadi University of Tétouan, Faculty of Sciences, Morocco*

[d] *SMAP (Surfaces and Porous Materials Group), Institute of Sustainable Processes, University of Valladolid, C/Dr. Mergelina, s/n, 47011, Valladolid, Spain*

[e] *Applied Physics Dept., ETSIIAA, University of Valladolid, Campus la Yutera, 34004, Palencia, Spain.*

**Corresponding authors*

E-mail addresses: m.douma@umi.ac.ma (M. Douma), a.bouazizi@umi.ac.ma (A. Bouazizi)

HIGHLIGHTS

- The effectiveness of Al-PILCs in adsorbing phenol from water was studied.
- Al-PILC exhibited a substantial rise in phenol adsorption compared to RC.
- ~~The~~ phenol was removed via π-π conjugation and electrostatic interaction.
- Al-PILC showed remarkable adsorption of polyphenols from Olive Mill Wastewater.
- Reuse efficiency of Al-PILC remained ~64% after 5 successive recycling steps.

ABSTRACT

An alumina-pillared clay (Al-PILC) has been synthesized and tested for its ability to adsorb phenol from aqueous solutions, and polyphenols from Olive Mill Wastewater (OMW). The synthesis

processes were investigated by varying parameters like the Al/clay ratio, with a molar ratio of [OH^-]/[Al^{3+}] = 2.4. Various techniques, including XRD, BET, XRF, FTIR, and SEM were used to characterize the resulting solids. The effect of key factors as pH, initial pollutant concentration, and contact time, were examined in order to evaluate the phenol adsorption capacities of raw clay (RC) and optimized Al-PILC$_{10}$ materials. The specific surface areas of RC and Al-PILC$_{10}$ were 40 and 127 m^2/g, respectively, resulting in increasing the phenol adsorbed quantity from 14.15 mg/g for RC to 30.61 mg/g for Al-PILC$_{10}$ clays, at pH 2 and 45 °C. Pseudo-second-order kinetics and ~~the~~ Freundlich adsorption isotherm were suitable for describing phenol adsorption on both clays. Furthermore, Al-PILC$_{10}$ exhibits an impressive removal efficiency of 76% for polyphenols from OMW, in contrast to the 50% achieved by RC at acidic pH. Furthermore, Al-PILC$_{10}$ showcased a superior desorption rate and a favorable regeneration capacity of 64% compared to RC (45%), even after multiple adsorption-desorption cycles. These findings emphasize the potential of pillared clay as a cost-effective adsorbent for the efficient removal of phenol and polyphenols from wastewater.

Keywords: Alumina-pillared clays; Adsorption; Phenol; Polyphenols; Olive Mill Wastewater.

1. Introduction

Phenol and its derivatives are crucial in the chemical industry, while showing properties that were initially not considered pollutants. However, as a result of incorrect utilization and subsequent release into the environment, these substances have escalated to harmful concentrations, resulting in the generation of toxic wastewater that presents considerable health hazards. This perilous waste is linked to conditions such as cancer, liver impairment, nausea, protein degradation, skin lesions, kidney malfunction, and nervous system debilitation, highlighting the critical need for intervention [1,2]. In several Mediterranean countries, such as Morocco, Tunisia, Greece, Spain, Turkey, and Italy, the production of olive oil is a key component of the agricultural economy [3–5]. The

effluents produced during the process of olive oil production exhibit a significant concentration of phenolic compounds, suspended organic matter, polyalcohols, organic acids, polysaccharides, lignin, and pectin [6]. These components contribute to high Chemical Oxygen Demand (COD) and Biological Oxygen Demand (BOD), making the untreated discharge of olive oil processing effluents a serious ecological threat to freshwater resources, soil, surface water, groundwater quality, and other ecosystems [4]. Olive polyphenols, which are distributed throughout both the water and oil phases of the extraction process, have an intriguing property. Despite their high polarity and solubility in water, a significant amount is missing from the wastewater. Polyphenols in olive mill wastewater (OMW), with concentrations typically ranging from 600 to 25000 mg/L [5], stand as primary valuable components that can be extracted, purified, and applied across various industries, including agri-food, pharmaceutical, and cosmetics [4,7]. Due to their strong natural antioxidant properties, numerous research underscores the benefits of phenolic substances and their recovery from depolyphenolized OMW, for example via mechanical pretreatment and a selective extraction process involving adsorption [6,8]. Similarly, other researchs ~~projects~~ have successfully demonstrated the OMW degradation. For example, Al-Qodah et al. [9] investigated the biodegradation of OMW with thermophilic bacteria, and a combined ultrasonic irradiation and aerobic biodegradation treatment in another study [10]. Furthermore, these findings emphasize promising avenues for the degradation of phenolic compounds in OMW.

Many studies have focused on removing and recovering phenolic compounds from OMW to address both their economic value and potential negative effects on treatment processes. Several methods, including liquid-liquid or liquid-solid extraction [6,8], chemical electrochemical oxidation [11,12], precipitation [13], membrane processes [14], ion exchange [15], extraction [16], biological processes [17], heterogeneous photocatalysis [18,19], distillation [20], and adsorption [5,21–23], have been employed to remove phenol and polyphenol from water. Although these

methods offer advantages, they also come with several drawbacks that limit their widespread application. These drawbacks include high operation costs, the production of poisonous by-products, high chemical consumption, complicated operational techniques, low efficiency, and the generation of toxic by-products [2]. In contrast, numerous studies have shown that the adsorption process holds promise as a technology for removing phenol and phenolic compounds from solutions. This method is considered advantageous due to its simplicity, effectiveness, reasonable energy consumption, and economical operation [24]. Additionally, the adsorption method allows for regeneration, washing, and reuse of the adsorbent for multiple cycles.

In this regard, the choice of adsorbent is crucial in various adsorption processes. Heydaripour et al. [25,26] demonstrated the excellent efficacy of porous magnetic RMF-grafted-chitosan (R-g-Ch) beads in adsorbing various polyphenols from water. Particularly, they exhibited high efficiency in removing phenol and 4-chlorophenol from aqueous solutions. Supong et al. [24] used a biomass-derived activated carbon as a viable alternative to the expensive commercial activated carbon to adsorb phenolic compounds from water. Additionally, Baig et al. [27] investigated the extensive use of graphene-based adsorbents for the removal of phenolic compounds. Clay is a highly sought-after material due to its extensive accessibility and cost-effectiveness. Its large surface area, highly porous structure, extraordinary ion exchange capacity, and exceptional thermal stability are some of its features [27]. Clay is also attractive for various applications due to its special capacity to simultaneously and efficiently absorb a wide range of contaminants [28].

Several researchers have employed clay material to eliminate phenol and polyphenol from water-based solutions. Activated clay was used in a study by Al-Malah et al. [29], and the results showed that hydrophobic interactions were mainly responsible for the sorption of phenolic content. Likewise, Chaari et al. [3] employed locally sourced natural clay as an inexpensive adsorbent to eliminate phenolic compounds from OMW, achieving an impressive efficiency rate of 79%. Lee

et al. [30] used of organo- and inorgano-organo-modified bentonite and locally collected clay to efficiently attenuate bisphenol A (BPA) from aqueous solutions. The results indicated that the BPA loading capacity was estimated at 50.976, 30.476, 19.586, and 10.086 mg/g for organo-modified bentonite, organo-modified locally collected clay, inorgano-organo-modified bentonite, and inorgano-organo-modified locally collected clay, respectively.

Montmorillonite (Mt) is natural clay that possesses adsorption abilities, although its capacity is limited. However, it is possible to enhance the adsorption properties of Mt by employing appropriate methods that increase the space between its layers. In a study conducted by Peng et al. [31] Mt and reduced charge montmorillonites (RCMs) were modified using Gemini surfactants, resulting in the expansion of interlayer space. Another study by Michaela et al. [32] conducted a study examining the use of magnetically modified Mt for the removal of Zn(II), Cd(II), and Pb(II) cations from leachates in metallurgical waste. The study showed how modifying Mt improves some characteristics, increasing its capacity to adsorb materials a property that has been shown to be useful in the treatment of wastewater. It should be noted that, pillared interlayered clays (PILCs) have indeed attracted significant interest due to their unique properties, including strong surface acidity, large specific surface area and excellent thermal stability. These features make PILCs valuable in various applications, particularly in the field of catalysis and adsorption. Metal-PILCs, including Al-PILCs [33], Zr-PILCs [34], Cr-PILCs [35], Si-PILCs [36], Fe-PILCs [37], and Ti-PILCs [38], are commonly produced by substituting the exchangeable cations within smectite clays with metal complex cations. Through calcination, these metal complexes are transformed into oxide pillars, effectively widening the gaps between the clay layers. By extending the distance between layers, this change improves the characteristics of the clay.

The Al-PILC are typically prepared using aluminum salts, and some researchers have shown a method by utilizing alternative aluminum sources like saline slags which're harmful waste products

from secondary aluminum production. Remarkably, Al-PILC materials with adsorption capacities have been produced by these alternate sources [39,40]. However, it's important to note that the effective way to synthesize alumina still involves starting with an aluminum salt. In an effort to create these materials, research efforts have mostly focused on adjusting synthesis variables in order to accurately customize the characteristics and microstructure of Al-PILC materials. Furthermore, these studies aim to produce solids, with improved porosity and specific surface areas by forming polycations [39,41–43]. In summary, Al-PILCs offer unique advantages such as a large specific surface area, strong surface acidity, and excellent thermal stability, make them highly desirable materials for adsorption and other high-temperature applications.

This study proposes an innovative approach using natural clay to synthesize alumina pillared montmorillonite clay for phenol removal from aqueous solutions. This clay is selected as an adsorbent for phenolic compounds due to its abundant availability across various regions of Morocco. Additionally, it can be easily modified or functionalized, coupled with its porous structure comprising micro, meso, and macro pores, enhances adsorption capacity and expedites phenol diffusion into the clay matrix. Several analytical methods were used to explore the physico-chemical properties of the adsorbents. The research evaluates the adsorption models and analyzes the impact of process parameters on the phenol adsorption phenomenon. Moreover, original RC and synthesized Al-PILC are comparatively tested for the adsorption of polyphenols from OMW, thus representing a comprehensive and practical real-world application.

2. Materials and methods

2.1. Starting materials

The clay used for the experiment study was collected from Nouwajriyen in the Fez region of Morocco. Clay sample was crushed, ground, and sieved. Various chemicals were employed in the experiments, including sodium chloride (99%, NaCl), aluminum chloride (99%, $AlCl_3.6H_2O$),

144 sodium hydroxide (98%, NaOH), hydrochloric acid (37%, HCl), silver nitrate (99%, $AgNO_3$), and
145 phenol (99%, C_6H_5OH), all of them were purchased from Sigma-Aldrich, and used as received,
146 without ~~undergoing~~ additional purification ~~processes~~. The OMW was collected from the olive mills
147 of Meknes, Morocco. ~~This sample is pivotal in this study, providing insight into the characteristics~~
148 ~~and potential treatment strategies for olive mill effluent in this specific geographic area~~. Moreover,
149 all solutions were prepared using deionized water.
150 2.2. Synthesis of alumina pillared clay
151 The natural clay employed in this study was transformed into sodium clay (NaC) prior to the
152 synthesis of pillared clay. To achieve this, the natural clay was dispersed in deionized water and
153 vigorously shaken for approximately 6 h. Following Stokes' law, clay particles smaller than 2 µm
154 were subsequently collected. The clay was then dispersed in a 1 M of NaCl solution and agitated
155 for 24 h at room temperature. The NaC was separated by centrifuging it after the full cation
156 exchange, and it was then properly cleaned with deionized water to guarantee that there were no
157 chloride ions present (as verified by the $AgNO_3$ test). The resulting NaC was dried at 80 °C. The
158 Al-PILCs were prepared following the conventional methodology described by Roca Jalil et al.
159 [41], as depicted in Fig. 1.
160 The pillaring oligocation was synthesized by gradually adding 0.5 M NaOH solution ~~drop by drop~~
161 into 0.2 M $AlCl_3.6H_2O$ solution. This addition is done drop by drop at a rate of 1 mL/min while
162 vigorously stirring the mixture at 60 °C. The aim was to achieve a final molar ratio of $[OH^-]/[Al^{3+}]$
163 equal to 2.4. The resulting solution was aged at 60 °C for 12 h with stirring, and the solution was
164 then added dropwise to deionized water containing 3 wt.% of NaC. When the supernatant solution
165 showed no chloride ions (as demonstrated by the reaction with $AgNO_3$ solution), the resultant
166 products were extracted by filtration and then washed with deionized water. The materials were
167 calcined for two hours at 500 °C after being dried at 60 °C. A total of four Al-PILCs were made

Comentado [JIC1]: I don´t understand which full cation exchange you refer to

with varying aluminum contents. For every gram of NaC, 5, 10, 15, and 20 mmol of aluminum were employed. These resulting Al-PILCs are labeled Al-PILC$_5$, Al-PILC$_{10}$, Al-PILC$_{15}$, and Al-PILC$_{20}$ respectively.

Fig. 1. Scheme of the Al-PILC manufacturing process.

2.3. Batch adsorption experiments

The adsorption experiments were conducted in the dark by combining a specified concentration of phenol solution with a lump of clay. Under continual stirring, the effects of absorbent mass, initial phenol concentration, contact time, temperature and solution pH were investigated. 30 mL flasks were used for adsorption isotherm studies. To establish the optimal operational parameters for adsorbing phenol solution and polyphenol from OMW, the flasks were sealed and then placed in a thermostatic water bath with a stirring rate set at 125 rpm. Different doses of prepared clay ranging from 0.02 to 0.22 g were added to 25.00 mL of solution. Furthermore, the pH of the solution was adjusted within the range of 2 to 12 using NaOH (0.1 M) and HCl (0.1 M). The temperature was set at 25, 35, and 45 °C. The initial concentrations of prepared phenol in solution ranged from 9.00 to 280.00 mg/L. To monitor changes in phenol and polyphenol concentrations over time, 4 mL samples of each solution were collected.

The pollutant adsorption efficiency was evaluated by determination of phenol removal (R (%)) using Eq. (1).

$$R(\%) = \frac{(C_o - C_e)}{C_o} \times 100 \quad (1)$$

Where, C_0 is the initial concentration of the phenol and C_e the concentration at equilibrium. The quantity of adsorbed phenol (qe (mg/g)) was calculated using the Eq. (2).

$$q_e = \frac{(C_o - C_e)V}{m} \quad (2)$$

Where, V is the volume of the phenol solution used and m the mass of the adsorbent.

2.4. Adsorption kinetics and isotherm modelling

The experimental results were fit using nonlinear kinetics, as well as isotherm models to ascertain the adsorption mechanism of phenol onto RC and Al-PILC clays. Adsorption kinetics was modelled by using pseudo-first order and pseudo-second order, whereas, isotherms were fitted to Langmuir, Freundlich and Redlich Peterson models, whose equations are summarized in Table Validity of the fitting ~~to such models~~ was confirmed by ~~the~~ error analysis calculations, such as the coefficient of determination (R^2), Chi-square analysis (χ^2) and the normalized standard deviation (Δq (%)).

Table 1. Kinetic and isotherm models.

The parameters in Table 1 are the following ones: q_e: adsorption capacity at equilibrium (mg/g), q_t: adsorption capacity at time t (mg/g), k_1: pseudo-first-order rate constant (1/min), k_2: pseudo-second-order rate constant (g/mg.min), k_{id}: intra-particle diffusion rate constant ($min^{1/2}$.mg/g), C: thickness of the boundary layer, C_e is the equilibrium concentration (mol/L), q_m is the maximum amount adsorbed for formation of a complete monolayer on the surface of the adsorbent (mg of pollutant/g of adsorbent), K_L is Langmuir constant related to the affinity of binding sites. K_F and n are Freundlich constants that express the capacity and the adsorption intensity, respectively and K_R and β ($0 < \beta < 1$) are the R-P constants.

2.5. Regeneration study

In order to evaluate the procedure's economic viability and look into the possibilities of reusing the adsorbent material, regeneration studies are crucial for every adsorption process. In the regeneration studies, 50 mg of clay samples were mixed with 50 mL of phenol solution at a concentration of 10^{-3} M. The mixture was stirred for 24 h to ensure maximum adsorption capacity.

To desorb the saturated clays, a solution containing 50% acetone and 50% NaOH was used, and the mixture was agitated for 2 h. The resulting solutions were filtered, washed, and dried at 105 °C in an oven. The regenerated clays were subsequently employed for adsorbing the test substance to evaluate their potential for reuse. Furthermore, the desorbed phenol was recovered by adjusting the pH of the solution to a slightly acidic level through the addition of HCl. This protonation process converts phenolate ions back into phenol. Subsequently, acetone and water were evaporated via a distillation process. Due to its higher boiling point compared to acetone and water, phenol remained in the reflux flask.

The regeneration rate (RR) was calculated using Eq. (3) after consecutive regeneration cycles.

$$\mathrm{RR}(\%) = \frac{C_{de}}{C_{ad}} \times 100 \quad (3)$$

2.6. Characterization methods and analysis

Various techniques and instruments used to analyze and characterize the prepared samples. X-ray diffraction (XRD) analysis was performed to assess the structural properties of the materials. XRD measurements were conducted using an X'PERT MPD-PRO wide-angle powder diffractometer with CuKα radiation (λ = 1.5406 Å). The scanning range spanned from 2° to 50° (2θ), with a step size of 0.02° and a scanning speed of 2° min^{-1}. The XRD spectra were obtained from oriented slides of the prepared samples. N_2 adsorption/desorption isotherms at 77 K and the relative pressure (P/P_0) range of 0.0-1.0 were used to examine the particle size distribution and specific surface area of the samples using equipment from Micromeritics ASAP 2010. BET (Brunner Emmett and Teller) theory was used to compute the specific surface area, while BJH (Barrett, Joyner, and Halenda) analysis determined the average pore diameter. X-ray fluorescence spectroscopy (XRF) on a dispersion wavelength spectrometer, model SRS 200, was employed to determine the chemical compositions. Fourier transform infrared spectrometry (FTIR) was performed using a Shimadzu,

JASCO 4100 spectrometer over the spectral range of 400 to 4000 cm^{-1} with a spectral resolution of 2 cm^{-1}. The morphology of the samples was observed using a JEOL JSM-IT500HR Scanning electron microscope (SEM) coupled to an energy dispersive X-ray spectroscopy (EDS) analysis. The point of zero charges (pH_{PZC}) is a useful parameter for characterizing the adsorbents because it represents the pH value at which the adsorbent's surface charge becomes neutral or zero. The determination of pH_{PZC} was performed according to the solid addition method described by Cardona et al. [39]. The pH_{PZC} value was determined from the curve that cuts the initial pH (pH_i) line of the pH_f–pH_i plot vs pH_i (being pH_f the final value of pH).

Phenol concentrations were analyzed using a Shimadzu UV-1240 spectrophotometer at 270 nm, while total polyphenol concentration were determined using the Folin–Ciocalteu technique described by Singleton and Ross in 1965 [44]. For polyphenols, 200 µl of each extract was mixed with a diluted Folin-Ciocalteu reagent and a sodium carbonate solution, followed by 30-minute incubation, and absorbance was measured at 765 nm. A calibration curve was concurrently prepared using gallic acid at different concentrations. This dual approach provided a comprehensive understanding of the changes in both phenol and polyphenol concentrations over time. In addition, the evaluation of OMW treatment involved the analysis of multiple parameters, including pH (measured using a HANNA HI1131 pH meter), conductivity (determined with an ADWA AD3000 Conductivity Meter), turbidity (measured with an optical HACH 2100N portable turbidimeter), chemical oxygen demand (COD), and biological oxygen demand (BOD_5). BOD_5 levels were assessed using an Oxi-Direct Lovibond BOD meter. COD determination relied on the oxidation of reducing substances through boiling (at 150 °C for 2 h) in the presence of an excess of potassium dichromate in an acidic environment (H_2SO_4). This process involved the addition of a catalyst (silver sulfate) and a complexing agent for chlorides (mercury sulfate). After the reaction,

COD levels were quantified by measuring the optical density of a properly diluted sample using spectrophotometry at a wavelength of 620 nm.

3. Results and discussion

3.1. Adsorbents characterization

Fig. 2a displays XRD patterns for RC, NaC, and Al-PILCs. These patterns offer insights into the composition of the samples, which consist of quartz (SiO_2), calcite ($Ca(CO_3)$), kaolinite ($Al_2Si_2O_5(OH)_4$), illite [$(K,H_3O)Al_2Si_3AlO_{10}(OH)_2$] and Mt. The XRD pattern of RC exhibits a distinct peak, indicating the presence of Mt, with a basal distance d_{001} of 15.02 Å. Considering that the thickness of an individual Mt layer is 9.6 Å, the interlayer space measures approximately 5.8 Å [45]. The observed change in the spectrum analysis of NaC involved a shift in the peak (001) position resulting in a decrease in the interreticular distance from 15.02 to 12.68 Å. This shift indicates an exchange process between sodium (Na) and calcium (Ca) and the obtained value (12.68 Å) is characteristic for a natural Mt containing mainly sodium cations in their interlayers [41].

Comentado [JIC2]: Why not including the chemical composition of Mt as done with illite or kaolinite?

The subsequent intercalation with Al_{13} cations leads to increased basal spacing to 18.00, 18.50, 18.20 and 18.10 Å for Al-PILC$_5$, Al-PILC$_{10}$, Al-PILC$_{15}$ and Al-PILC$_{20}$ respectively. These increments suggest an interlayer separation of around 9 Å. This value aligns with the average diameter of Keggin Al_{13} cation particles (9 Å), providing evidence of a successful Al_{13} intercalation into Mt. A comparison of the range of angles (from 4° to 8°) across different samples shows no significant differences in peak width, according to the data shown in Fig. 2b. Notably, Al-PILC$_{10}$ stands out among these samples, exhibiting the greatest basal distance and a distinctly sharper and more intense peak. This observation implies a higher level of homogeneity in the intercalation process within this particular sample. Conversely, the presence of less intense and broader peaks

suggests the possibility that a portion of the Mt clay either remained unpillared or experienced delamination [46].

Fig. 2c displays the N_2 adsorption-desorption isotherms at 77 K for both the RC and Al-PILCs adsorbents. According to the IUPAC classification system [45], the isotherms exhibit a type IV pattern for both RC and Al-PILCs with varying concentrations of aluminum. This pattern suggests the presence of a heterogeneous solid structure characterized by micro and mesopores. All samples demonstrate hysteresis of the H_3 type, indicating the presence of particle agglomerates with slit-shaped pores that undergo capillary condensation [37]. Notably, the RC exhibits lower N_2 adsorption at low relative pressures compared to Al-PILCs, indicating a lesser contribution from micropores [47]. Table 2 presents the structural properties obtained from the N_2 adsorption-desorption isotherms.

Table 2. Micropore structure parameters of RC and synthesized Al-PILCs.

Based on the presented data, it is evident that there is an increase in the specific surface area (S_{BET}) and total pore volume for all Al-PILCs compared to the RC. Furthermore, the results indicate that the pillaring process leads to the formation of a larger number of micropores, which contribute significantly to the observed increase in specific surface area (S_{BET}) from 40 to 141 m^2/g. Additionally, compared to the Al-PILC$_5$, Al-PILC$_{10}$, and Al-PILC$_{15}$ samples, the Al-PILC$_{20}$ sample has the highest value for total pore volume, indicating a greater contribution from micropores in this sample. Typically, when aluminum is utilized in the pillaring process, there's a significant alteration in the properties of the solids, contrasting with the initial state of the clay. These transformations entail a significant increase in the overall specific surface area, micropore volume, and microporous area. It ought to be mentioned that ~~the~~ sorption is a process influenced by many factors. A higher specific surface provides a larger surface of interaction with the solution, which

promotes adsorption. But the appropriate size pores can allow selective adsorption depending on the size of the molecules present in the phenol. These physic-chemical parameters often interact in a complex way. In this regard, and considering the XRD findings, the RC and Al-PILC$_{10}$ specimens have been chosen for more extensive characterization and comparison of their outputs in phenol and OMW adsorption studies.

The chemical composition of the RC and Al-PILC$_{10}$ clays, as obtained from XRF, is reported in Table 3. The analysis shows that the used clay primarily consists of natural alumina-silica, with SiO_2 (42.46 wt.%) and Al_2O_3 (14.15 wt.%). The SiO_2/Al_2O_3 ratio of RC is approximately 2.98, falling within the range of [2.5-3]. This ratio suggests that the clay used is predominantly composed of smectite, specifically the Mt family, which is consistent with the findings of Dobe et al. [33]. Furthermore, the presence of CaO is significant in RC, accounting for 12.12 wt.% and indicating the presence of calcium primarily from carbonates. Additionally, there are traces of sodium, phosphate, potassium, manganese, and titanium oxides as impurities. The results of the chemical composition analysis of Al-PILC$_{10}$ demonstrate an increase in Al_2O_3 content and a decrease in CaO content due to the substitution of Ca and Na during preparation. This finding suggests that aluminum is inserted into the interlayer space as pillars [33].

Table 3. Chemical composition of RC and Al-PILC$_{10}$.

Fig. 2d presents the FTIR spectra of Al-PILC$_{10}$ and RC. Although many of the peaks in both spectra are identical. The occurrence of two peaks in the OH stretching region at 3440 and 3625 cm^{-1} is a common characteristic of water molecules on the surface of clays and O-H stretching bonded with Al^{3+} cations respectively. In addition, the presence of a peak at 1634 cm^{-1} indicates the occurrence of water bending vibration. The band seen at 1413 cm^{-1} is related to the carbonate group (CO_3^{2-}) elongation vibrations. The broad peak observed at 1034 cm^{-1} can be attributed to the in-plane

stretching vibration of surface Si-O-Si bonds. In the FTIR spectra of Al-PILC$_{10}$, a noticeable increase in the intensity ratio between the peaks at 3625 and 3440 cm^{-1} compared to that of the RC. The increase in intensity of the 3440 cm^{-1} peak may be due to the formation of silanol groups resulting from the breaking of Si-O-Al bonds in the tetrahedral layer [48]. It should be noted that, the enhanced intensity of the peak at 3440 cm^{-1} could be attributed to the generation of silanol groups, which occur as a result of the disruption of Si-O-Al bonds within the tetrahedral layer. A reaction between the Al_{13} pillar and the protonated Si–OH–Al linkage results in the formation of either Si-tetrahedral–O–Al pillar or Al-tetrahedral–O–Al pillar linkages [48]. These connections show that the Al pillar successfully formed between the clay layers. The three bands recorded at 678, 524 and 471 cm^{-1} correspond to the deformation vibrations of Si-O-(Al; Mg; Fe) bonds, and the band at 784 cm^{-1} was attributed to Quartz. Furthermore, it should be noted that these observations are consistent with the obtained results from XRD analysis.

Fig. 2. (a) XRD patterns of RC, NaC, and Al-PILCs, (b) Comparison of XRD patterns of Al-PILCs, (c) N_2 adsorption–desorption isotherms of RC and Al-PILCs, (d) FTIR spectra of RC and Al-PILC$_{10}$.

The changes in the surface morphology and elemental composition of the RC and Al-PILC$_{10}$ clays are illustrated in Fig. 3. The surface morphology of RC (Fig. 3a) is massive, agglomerated and consists of large aggregates of particles with smooth surfaces. However, following the intercalation process, the clay transforms into a more porous and airy consistency (Fig. 3c). The same observation was made by Cardona et al. [39], which further supports the findings. The uniform morphology is attributed to a decrease in face-to-face aggregations and an increase in face-to-face interactions. The samples show many relatively small particles and more relatively flat plates. The EDX examination of RC (Fig. 3b) shows the existence of O (52.24 wt.%), C (11.38 wt.%), Si (8.23

wt.%) and Al (3.65 wt.%). However, after pillaring with Al_{13} (Fig. 3d), the composition changed to O (49.71 wt.%), C (4.69 wt.%), Si (21.11 wt.%) and Al (18.85 wt.%). The EDX spectra indicate a significant increase in aluminum and a reduction in carbon. Moreover, the Al/Si ratios of 0.44 and 0.89 are observed for RC and Al-PILC$_{10}$ clays, respectively, reflecting the extent of aluminum integration. This implies an elevation in the Al/Si ratio owing to the presence of aluminum polycations within the interlayer space, as reported by León et al. [49].

Fig. 3. SEM images of (a) RC and (c) Al-PILC$_{10}$, EDX spectrum of (b) RC and (d) Al-PILC$_{10}$.

The pH_{pzc} is a crucial parameter in understanding the surface charge of adsorbents and its significance in adsorption process. The pH_{pzc} values of RC and Al-PILC$_{10}$ clays are illustrated in Fig. 4, where the RC exhibited a pH_{pzc} of 7.44, while the Al-PILC$_{10}$ had a pH_{pzc} of 5.81. These discrepancies may stem from the introduction of acid sites into the clay via the intercalated Al_{13} polycations [41]. Consequently, it can be inferred that the surface of the specimens will possess a positive charge until the pH drops below the pH_{pzc}. At the pH_{pzc}, the surface charge will become neutral, and beyond the pH_{pzc}, it will transition to a negative charge.

Fig. 4. Determination of the pH_{PZC} for RC and Al-PILC$_{10}$.

3.2. Phenol adsorption onto RC and Al-PILC$_{10}$

3.2.1. Adsorption tests and comparative study

An analysis of the phenol adsorption of each prepared samples was done to validate the choice of Al-PILC$_{10}$ as the ideal dosage. Fig. 5 illustrates the rejection of phenol as a function of various Al/clay ratios. It was found that different Al/clay ratios changed the effectiveness of phenol removal by both RC and Al-PILCs. Among all the samples, Al-PILC$_{10}$ exhibited the highest performance, reaching 62% phenol removal rate. Furthermore, it was discovered that the interlayer

spacing was the main variable affecting how well phenol adsorbs on the adsorbents. However, it is crucial to remember that interlayer space is not the only factor.

It should be noted that, the existence of micropores could present difficulties by potentially restricting phenol molecules from accessing particular adsorption sites, resulting in a decrease in the overall adsorption capacity of the system [21]. Thorough a comprehensive analysis, it was also observed that Al-PILC$_{10}$ showed the best correlation between pore size and surface characteristics. Based on these findings, it can be concluded that Al-PILC$_{10}$ is the optimal choice for optimizing the adsorption parameters.

Fig. 5. Rejection of phenol as a function of different Al/clay ratios.

3.2.2. Optimization of batch adsorption parameters

Effects of pH

Fig. 6a exhibits the effect of pH on phenol adsorption. It can be observed that, the amount of phenol adsorbed is seen to decrease with increasing pH, suggesting that an acidic environment is more conducive to phenol adsorption onto RC and Al-PILC$_{10}$ clay. At a pH lower than the pKa value of phenol (9.89), the phenol molecule remains in their undissociated form [31]. Similarly, the two adsorbents exhibit positive charges on their surfaces at pH values lower than their respective pH_{pzc} values (7.44 and 5.81). Consequently, the positively charged adsorbents and the uncharged phenol molecules are mutually attracted to each other within this pH range, leading to improved efficiency in the removal of phenol. In basic environment, the decrease of adsorption is caused by electrostatic repulsive forces between negative charges of the RC and Al-PILC$_{10}$ surfaces (at $pH > pH_{pzc}$) and the phenolate anions, as well as between the phenolate ions themselves (at pH > pKa). Indeed, the surface functions of the RC or Al-PILC$_{10}$ and the phenol molecules are both dissociated and negatively charged with the predominance of conjugated forms of the bases [39]. Additionally, it

396 is observed across all pH ranges, Al-PILC$_{10}$ adsorbed more phenol than RC. The disparities in
397 adsorption capacity between Al-PILC$_{10}$ and RC can be attributed to the electrostatic interaction
398 between phenol molecules and the micropores present in Al-PILC$_{10}$ [39,41]. This effect highlights
399 how the pillaring process alters the surface chemical properties of RC, consequently affecting its
400 adsorption capabilities. Furthermore, this demonstrates how surface chemistry has a major impact
401 on how organic compounds are adsorbed, as confirmed by Peng et al. [31]. As the adsorption of
402 phenol exhibits a maximum adsorbed quantity at pH 2, it was chosen for the subsequent adsorption
403 experiments.
404 Effect of clay mass
405 Fig. 6 illustrate how varying the mass of RC and Al-PILC$_{10}$ clays influences the adsorption process.
406 The findings indicate that the percentage of adsorption increases as the amount of adsorbent does
407 which is attributed to the greater number of available reaction sites. While, the adsorption capacity
408 (in terms of adsorbed mass per unit of adsorbent mass) decreases, since the accumulation of a large
409 number of adsorbents reduces the effective utilization of adsorption sites, [33]. It should be noted
410 that, for all adsorbent masses tested, the Al-PILC$_{10}$ clay (Fig. 6c) exhibits a significantly higher
411 rate of phenol removal (up to 50 %) compared to RC (Fig. 6b), less than 30%. This discrepancy is
412 likely due to the higher surface area and the presence of more active adsorption sites in Al-PILC.
413 Additionally, it was observed that100 mg seems to be an optimal mass, for both RC and Al-PILC$_{10}$
414 clays, achieving an equilibrium between increase of adsorption percentage and decrease of
415 adsorption capacity. This rapid attainment of equilibrium can be attributed to the abundance of
416 active sites on the clay surface and/or the mineralogical composition [50].

417 Fig. 6. (a) pH effect on the phenol adsorbed quantity on the RC and Al-PILC$_{10}$ clays, and the
418 impact of clay mass on the phenol adsorbed quantity for (b) RC and (c) Al-PILC$_{10}$.

3.3. Adsorption kinetics and isotherm modelling

3.3.1. Adsorption kinetic

Fig. 7 illustrates the impact of contact time on phenol adsorption using RC and Al-PILC$_{10}$ samples at various temperatures (25, 35 and 45 °C). Based on the figure, the amount of adsorbed phenol on both adsorbents rises as the contact time increases, reaching a maximum level after approximately 60 min. Because there are a lot of empty active sites on the surface of the adsorbents, the early phases show a fast rate of adsorption. As the process progresses, the rate slows due to factors like the reduction of phenol concentration and the formation of aggregates occupying active sites [31,51]. Notably, the maximum capacities (q_e) of phenol obtained are 9.89 and 20.23 mg/g for RC and Al-PILC$_{10}$, respectively. The pillaring clay process, particularly with Al-PILC$_{10}$, create more active sites, enhancing the adsorption capacity and demonstrating a higher affinity for phenol by expanding the interlamellar space in the clay structure [33].

Fig.7a and Fig.7b ~~present~~ also plot ~~depicting~~ the application of the pseudo-first-order and pseudo-second-order kinetic models to the adsorption of phenol by RC and Al-PILC$_{10}$ clays, respectively. Additionally, Table 4 provides a summary of the fitting parameters associated with each kinetic model. The results demonstrate that the pseudo-second-order kinetic model exhibits a high correlation coefficient ($R^2 \approx 0.99$), close to 1, for both clays (Fig. 7 and Table 4). This indicates that the pseudo-second-order model is more suitable for explaining the adsorption of phenol by the adsorbents compared to the pseudo-first-order model. The calculated value (q_{e2}) from the pseudo-second-order kinetic model is in closer agreement with the experimental value (q_{exp}) compared to the pseudo-first-order equation. Consequently, the pseudo-second order provides the most accurate representation of the experimental phenol adsorption data for both RC and Al-PILC$_{10}$ at all three temperatures [52–54]**.**

Table 4. Kinetic parameters of Phenol adsorption at different temperatures onto RC and Al-PILC$_{10}$.

While first and second-order fitting models give an overall picture of the absorption process, we can get insight on the mass transfer process of phenol at the solid-liquid interface by using the intra-particle diffusion model. The model, represented in Fig.7c and Fig.7d for phenol adsorption on RC and Al-PILC$_{10}$ samples, reveals two distinct stages. The first stage of adsorption is governed by boundary layer diffusion, while the final stage is attributed to intra-particle diffusion of phenol molecules [24]. The rate of intra-particle diffusion decreases during the final stage, as evidenced by the greater intra-particle diffusion rate constant K_1 compared to K_2 (Table 5). This decline is attributed to pore blockage and steric repulsion caused by adsorbed phenol on the surface of both adsorbents. In that sense it can be commented that RC, at 25 ºC gives the lower decline but this is since also these conditions result in one of the lowest adsorption constant values (C_1 and C_2). The non-intersecting plots with the origin suggest that the adsorption process is not solely limited by intra-particle diffusion, but also influenced by other kinetic mechanisms.

Fig. 7. Kinetics of phenol adsorption on (a) RC and (b) Al-PILC$_{10}$; Intra-particle diffusion model for Phenol adsorption on (c) RC and (d) Al-PILC$_{10}$.

Table 5. Parameters of the intra-particle diffusion model equations.

3.3.2. Adsorption isotherms

Optimizing the design of an adsorption system requires a thorough understanding of the distribution of the adsorbate. Three equilibrium isotherm equations, namely Langmuir, Freundlich,

and Redlich-Peterson, were used in this investigation to explain how phenol sorption occurred on various adsorbents. The resulting isotherms, along with their corresponding fits, are presented in Fig. 8. The increase in the adsorption capacity of RC and Al-PILC$_{10}$ as the phenol concentration increases may be due to a higher probability of collision between the pollutant and the adsorbent [22]. The obtained parameters from the isotherm models, along with the chi-squared value (χ^2), are summarized in Table 6. The Langmuir isotherm suggests a monolayer formation of adsorbate molecules on the adsorbent surface, with identical adsorption sites of equivalent energy. In contrast, the Freundlich model describes a multisite adsorption isotherm, accounting for sorption on surfaces with varying affinities or heterogeneous surfaces [55]. The Redlich-Peterson model, blending characteristics of both Langmuir and Freundlich models, offers a middle ground [56]. Examination of the determination coefficient (R^2) values reveals that both Freundlich and Redlich-Peterson models aptly characterize the experimental data for both samples. This assertion is further supported by the observation of low $\chi 2$ and β values in comparison to the Langmuir model. Since the Langmuir equation requires a homogenous surface, the fact that the Langmuir isotherm does not fit the actual data very well because there is not a homogeneous distribution of active sites on the surface of both adsorbents [23]. Also Fig. 8 shows that Freundlich and Redlich-Peterson fitting match almost perfectly, suggesting that last one is clearly displaced to multisite adsorption. Considering the shape of the isotherms, the Freundlich model is found to be the most suitable for describing phenol adsorption on RC and Al-PILC$_{10}$ across all temperature and concentration ranges, it suggests that the adsorption process is probably affected by variables such as surface heterogeneity, the formation of multiple layers during adsorption, and non-uniform distribution of adsorption sites on the adsorbents surface. The increasing K_F values and the 1/n parameter less than one indicate a strong affinity of the adsorbent for phenol and the adsorption process is favorable. The pillared clay demonstrates higher phenol adsorption capacities than the RC due to three main

differences: increased hydrophobicity, lower pH_{PZC}, and an enhanced microporous structure. The enhanced hydrophobicity of the pillared clay enhances its selectivity for organic molecules, making it more effective than natural mineral clay [41].

Fig. 8. Adsorption isotherms of phenol on RC, and Al-$PILC_{10}$ at different temperatures ((a,d):25 °C; (b,e): 35 °C; (c,f): 45 °C) with nonlinear regression of Langmuir, Freundlich and Redlich-Peterson models.

Table 6. Model parameters for phenol adsorption on RC and Al-$PILC_{10}$ at different temperatures.

3.4. Thermodynamic study

To study the thermodynamic behavior of the phenol adsorption onto RC and Al-$PILC_{10}$ adsorbents, the thermodynamic parameters (ΔH°, ΔS°, and ΔG°) were calculated using the following equations (Eq. (4) and Eq. (5)) [51]:

$$ln\, K_F = -\frac{\Delta H^\circ}{RT} + \frac{\Delta S^\circ}{R} \quad (4)$$

$$\Delta G^\circ = \Delta H^\circ - T\Delta S^\circ \quad (5)$$

Where K_F (L/mg) is the Freundlich isotherm constant, T (K) is the absolute solution temperature, and R ~~(8.314 J/mol. K)~~ is the universal gas constant.

The obtained thermodynamic parameters are presented in Table 7. The values of ΔH° determined for phenol adsorption onto RC and Al-$PILC_{10}$ were 31.88 and 22.64 kJ/mol, respectively. Positive ΔH° values indicate endothermic adsorption process [41], while values less than 40 kJ/mol suggest physisorption, signifying weak attraction between phenol and the adsorbent surfaces [56]. The positive ΔS° values suggest an increase in randomness at the solid/solution interface during the adsorption process [24], indicating that phenol molecules display a higher degree of disorder on the RC surface compared to Al-$PILC_{10}$. This finding highlights the differences in phenol molecule

structural organization between these two adsorbents. However, the negative ΔG° values signify the spontaneity of the adsorption process, with decreasing values as higher temperature rises suggests a more favorable process. This pattern demonstrates the increasing thermodynamic favorability of adsorption as temperature rises [47]. Similarly,

adsorption is clearly more favorable for Al-PILC$_{10}$ than for RC.

Table 7. Thermodynamic parameters of phenol adsorption by RC and Al-PILC$_{10}$.

3.5. Adsorption mechanism

Fig. 9 displays the FTIR spectra of both RC and Al-PILC$_{10}$ (those of Fig. 4), along with the spectra of phenol and that of RC (Fig. 9a) and Al-PILC$_{10}$ (Fig. 9b) after being saturated in phenol. The post-adsorption spectra reveal new vibration bands, notably at 2943 and 2850 cm^{-1}, corresponding to aromatic C-H vibrations and at 1397 cm^{-1} attributed to the C-O group of phenol ~~(Fig. 9)~~. These results confirm the presence of phenol and its adsorption on both RC and Al-PILC$_{10}$ clays. While many peaks in both spectra are identical, such as Al−O, Si−O, and Si−O−Si, differences emerge in the OH-stretching at 3430 cm^{-1} yet commented in Fig. 4.

Based on the kinetic, isotherm, thermodynamic and FTIR results, ~~revealed that~~ phenol adsorption was considered primarily physical, but due to the complexity of the process, diverse interaction mechanisms exist [57], acting on the adsorption of phenol. These include the electrostatic attraction, π-π conjugation effect, host-guest interaction, and hydrogen bonding.

Comentado [JIC3]: You commented 3 mechanisms but next you include four possible ones.

Specifically, a π-π conjugation effect occurs between the π system on the RC or Al-PILC$_{10}$ surface, and the benzene ring phenol molecules [5,52,54]. The electrostatic interaction occurred considering the pKa of the adsorbate, the phenol will be attracted to the micropores present in Al-PILC$_{10}$ more than RC [5]. Furthermore, the adsorbent's surface oxygen-containing functional group has an intermolecular interaction force with phenol, which results in electrostatic attraction.

The phenomenon of hydrogen bonding enables the hydroxyl (-OH) groups present in both the adsorbent and phenol to interact with each other, as noted in prior research [58]. This interaction occurs as a result of the attractive forces between the hydrogen atoms of one -OH group and the oxygen atoms of another, facilitating a strong bond. Additionally, in the context of electron donor-acceptor interaction, the aromatic rings of phenolic compounds engage with the hydroxyl functional groups (-OH) found in both RC and Al-PILC$_{10}$. This interaction mechanism involves the electron-rich aromatic rings acting as donors, while the hydroxyl groups serve as acceptors, fostering a cohesive interaction between the adsorbent and the phenolic compounds.

Besides, macropores are also used as molecular transmission channels to reduce the resistance of diffusion, thereby enhancing the adsorption rate and capacity.

Fig. 9. FTIR spectra of (a) RC and (b) Al-PILC$_{10}$ before and after adsorption, alogn with pure phenol spectra.

3.6. Treatment of OMW through adsorption

RC and Al-PILC$_{10}$ were selected to compare the capacity as adsorbents for removal of polyphenols from OMW. According to data presented in Table 8, the initial pH of the OMW was ~~recorded at~~ 4.52. Following treatment, there was an increase in pH, attributed in part to a significant reduction in polyphenol content (from an initial values of 334.72 mg/L to 166.84 mg/L for RC and to 80.30 mg/L for Al-PILC$_{10}$) and a moderate decrease in organic matter, as evidenced by lower COD concentrations, primarily composed of organic acids [3,4,7]. A reduction in dissolved salt concentration was indicated by a decrease in conductivity post-treatment, from 16.22 to 14.03 mS/Cm (for RC) and 11.92 mS/Cm (for Al-PILC$_{10}$). Initially, the sample appeared cloudy with a turbidity of approximately 1930 NTU. After undergoing treatment, RC exhibited a 40% decrease in turbidity, while Al-PILC$_{10}$ showed a more pronounced reduction of 64%, suggesting a notable

558 decline in suspended particles, including organic constituents. The reduction in COD and BOD_5
559 can be attributed to the adsorption of high molecular weight organic molecules present in the olive
560 mill effluent onto RC and Al-$PILC_{10}$ [3,4,7].

561 Table 8. OMW characterization before and after treatment using RC and Al-$PILC_{10}$.

562 The efficiency of polyphenol removal on clay samples rises from 29 to 50% for RC and from 47
563 to 76% for Al-$PILC_{10}$ as the adsorbent dosage increases from 20 to 220 mg (Fig. 10a). This
564 phenomenon could be attributed to the increased availability of active surface sites for adsorption.
565 Fig. 10b depicts the impact of pH on the adsorption of polyphenols. It is evident that the removal
566 efficiency of polyphenols decreases as the pH increases, indicating that the adsorption of
567 polyphenol onto RC and Al-$PILC_{10}$ clays is more favorable in an acidic environment. At a pH
568 lower than the pKa value of phenol, the phenol molecule remains in its undissociated form [31],
569 mirroring the behavior observed during phenol adsorption in aqueous solution. Similarly, both
570 adsorbents exhibit positive charges on their surfaces at pH values lower than their respective pHpzc
571 values. Consequently, the positively charged adsorbents and the uncharged polyphenol molecules
572 are mutually attracted to each other within this pH range, resulting in improved efficiency in phenol
573 removal. Additionally, across all pH ranges, Al-$PILC_{10}$ adsorbs more phenol than RC. Fig. 10c
574 shows that equilibrium adsorption of OMW phenolic compounds occurred within 60 minutes,
575 resulting in removal efficiencies of approximately 45% for RC and 73% for Al-$PILC_{10}$. This
576 phenomenon can be attributed to the significant driving force provided by unoccupied active sites
577 on the adsorbent surfaces. Because of the endothermic nature of the adsorption process, increasing
578 the temperature resulted in higher adsorption yields, as shown in Fig. 10d. This increase is due to
579 stronger adsorptive forces between phenolic compounds and clay active sites. The differences in
580 removal efficiencies between Al-$PILC_{10}$ and RC can be attributed to electrostatic interactions

between phenolic compound molecules and Al-PILC$_{10}$ micropores. The material's large surface area amplifies these interactions, resulting in a significant increase in overall adsorption efficiency, particularly for polyphenol removal. Furthermore, the precisely defined chemical composition of Al-PILC$_{10}$, with specific bonding sites, is critical in establishing a strong binding affinity with polyphenols, contributing significantly to its outstanding performance as a polyphenol adsorbent. The findings presented in this section provide critical insights into the efficacy of our approach in addressing environmental challenges associated with olive oil mills, demonstrating its potential for treating effluents from other industries such as chemical production, metallurgy, and textiles.

Fig. 10. (a) Effect of adsorbent amount, (b) initial solution pH, (c) contact time and (d) temperature on the adsorption of polyphenol onto RC and Al-PILC$_{10}$.

3.6. Regeneration and reuse of spent clays

Fig. 11a illustrates the influence of regeneration on the adsorption capacity of both samples concerning phenol removal. After undergoing five cycles, the decrease in phenol removal efficiency was below 23% for both samples. Specifically, for RC and Al-PILC$_{10}$, the efficiency decreased from 67% and 84% to 45% and 64%, respectively. This suggests favorable regeneration capabilities for the adsorbents, allowing repeated use for phenol adsorption. Across all reusage cycles, Al-PILC$_{10}$ demonstrated superior adsorption performance and a higher desorption rate compared to RC. This indicates that pillared clay maintains high efficiency and notable regeneration capacity, making it a promising choice for repeated phenol adsorption applications. Furthermore, it's worth noting that the superior performance of the Al-PILC$_{10}$ is not only reflected in its higher desorption rate but also in its extended lifespan. This means that even after the five adsorption-desorption cycles, the pillared clay continues to exhibit exceptional adsorption performance, outperforming the other sample in terms of phenol removal. This extended

operational life and robust regeneration potential make the pillared clay an excellent choice for sustainable phenol adsorption processes, contributing to both environmental and economic benefits.

Fig. 11b displays the FTIR spectra of pure phenol and phenol recovered after desorption. According to this figure, it is evident that the characteristic peaks associated with the vibrational modes of functional groups in phenol, generally remain unchanged in terms of position and intensity in the extracted phenol compared to the pure one. This suggests that the extraction process did not induce significant changes in the molecular structure of phenol. Furthermore, this observation implies that the extracted phenol retains its initial molecular properties, which could be crucial for specific applications.

Fig. 11. (a) Regeneration test for phenol adsorption on RC and Al-PILC$_{10}$, (b) FTIR spectra of pure and extracted phenol.

Noted that spent materials RC and Al-PILC$_{10}$ can be used to improve the adsorption capacity of composite materials like polymer matrices. Their incorporation into building materials not only prevents absorbed contaminants from seeping into the environment but also, provides a sustainable disposal option while simultaneously improving material qualities.

Comentado [JIC4]: Thes asserts are not part of your research, so, in my opinion you cannot include here.

For example, the use of pillared clays in conjunction with biological treatments aids in the cleanup of phenolic compound-contaminated locations by the absorption of pollutants, which acts as a carbon source to promote microbial breakdown. In other words, their multifaceted utility extends from material enhancement to environmental remediation, presenting promising avenues for future research and applications [59].

4. Conclusion

In this study, Al-PILC was synthesized from Moroccan clay while varying the Al/clay ratio, for phenol and polyphenol removal. Characterization experiments confirmed the successful pillaring of the Moroccan raw clay and highlighted significant changes in its porous, chemical, and crystalline properties. The following main results were obtained:

- Materials with higher aluminum content had smaller pore sizes. The pore-tuning properties of aluminum additives and partial pore occupation resulted in a more organized pore size distribution in Al-PILC$_{10}$.
- Kinetic and equilibrium adsorption experiments identified the Freundlich isotherm and pseudo-second-order models as optimal for both clays, with adsorption capacities of 14.15 and 30.61 mg/g, for RC and Al-PILC$_{10}$ respectively. Additionally, the phenol adsorption processes were found to be endothermic and physical.
- Phenol was not easily released after adsorption, and the main adsorption mechanisms were electrostatic attraction, π-π conjugation effect, host-guest interaction, and hydrogen bonding. Furthermore, the differences in adsorption capacity between Al-PILC$_{10}$ and RC were attributed to electrostatic interactions between the adsorbent surface and pollutant species in solution, and interactions of species with Al-PILC micropores.
- The effects of external factors such as pH on adsorption mechanisms are not well comprehended. More thorough exploration is necessary to clarify how these factors impact the adsorption of phenol, to enhance the efficiency of Al-PILC in wastewater treatment.
- The results obtained clearly demonstrate that the optimal alumina pillared clay (Al-PILC$_{10}$) achieves notable reductions in turbidity, COD, BOD$_5$, and polyphenols levels in OMW compared to RC. This improvement is attributed to the substantial alteration in the surface

area of Al-PILC$_{10}$ adsorbent, resulting in a significant increase in overall adsorption efficiency, particularly in the removal of polyphenols.

- A promising regeneration method for this adsorbent was developed, utilizing a combination of acetone and NaOH desorption. This method produced high phenol desorption rates, up to 84% for Al-PILC$_{10}$, enhancing the sustainability of material.

Based on our results, we can envisage some recommendations for future research:

- Investigate synergies by combining adsorption with other treatment methods like membrane filtration to enhance phenol compound removal.
- To better understand molecular interactions, investigate the fundamental mechanisms of adsorption on natural RC and Al-PILC using methods such as DFT calculations or molecular dynamics simulations.
- Examine the viability and effectiveness of the RC and Al-PILC adsorbents in the treatment of other wastewaters from textile, pharmaceutical, and petrochemical sectors.
- Explore innovative techniques for treating and recycling these spent adsorbents to prevent the transfer of pollution to other environmental mediums, while conducting comprehensive life cycle assessments to inform decisions toward more sustainable practices.

References

[1] P. Palencia, J.M. Rowcliffe, J. Vicente, P. Acevedo, Assessing the camera trap methodologies used to estimate density of unmarked populations, J. Appl. Ecol. 58 (2021) 1583–1592. https://doi.org/10.1111/1365-2664.13913.

669 [2] H.A. Abdel-Gawwad, M.S. Ahmed, A.H. Mohammed, M. Badawi, A. Bonilla-Petriciolet,
670 E.C. Lima, Y.F. Salama, M. Mobarak, M.K. Seliem, Utilization of red clay brick waste in
671 the green preparation of an efficient porous nanocomposite for phenol adsorption:
672 Characterization, experiments and statistical physics treatment, Sustain. Chem. Pharm. 32
673 (2023) 1–14. https://doi.org/10.1016/j.scp.2023.101027.

674 [3] I. Chaari, A. Touil, M. Medhioub, Adsorption-desorption of phenolic compounds from
675 olive mills wastewater using Tunisian natural clay, Chinese J. Chem. Eng. 40 (2021) 287–
676 292. https://doi.org/10.1016/j.cjche.2020.12.020.

677 [4] A. Benamar, F.Z. Mahjoubi, N. Barka, F. Kzaiber, K. Boutoial, G.A.M. Ali, A. Oussama,
678 Olive mill wastewater treatment using infiltration percolation in column followed by
679 aerobic biological treatment, SN Appl. Sci. 2 (2020) 1–12. https://doi.org/10.1007/s42452-
680 020-2481-1.

681 [5] K. Yuney, A.A. Oladipo, M. Gazi, D.Z. Younis, CuO coated olive cake nanocomposites
682 for rapid phenol removal and effective discoloration of high strength olive mill wastewater,
683 Chemosphere. 253 (2020) 126703. https://doi.org/10.1016/j.chemosphere.2020.126703.

684 [6] Z. Al-Qodah, H. Al-Zoubi, B. Hudaib, W. Omar, M. Soleimani, S. Abu-Romman, Z.
685 Frontistis, Sustainable vs. Conventional Approach for Olive Oil Wastewater Management:
686 A Review of the State of the Art, Water (Switzerland). 14 (2022).
687 https://doi.org/10.3390/w14111695.

688 [7] Y. Dehmani, A. Ed-Dra, O. Zennouhi, A. Bouymajane, F. Rhazi Filali, L. Nassiri, S.
689 Abouarnadasse, Chemical characterization and adsorption of oil mill wastewater on
690 Moroccan clay in order to be used in the agricultural field, Heliyon. 6 (2020) e03164.

https://doi.org/10.1016/j.heliyon.2020.e03164.

[8] M.J. Fernandes, J. Gomes, P. Carvalho, R.C. Martins, E. Domingues, Removal and recovery of phenolic compounds from OMW by a cationic resin, Chem. Eng. Sci. 291 (2024). https://doi.org/10.1016/j.ces.2024.119925.

[9] Z. Al-Qodah, M. Al-Shannag, K. Bani-Melhem, E. Assirey, K. Alananbeh, N. Bouqellah, Biodegradation of olive mills wastewater using thermophilic bacteria, Desalin. Water Treat. 56 (2015) 1908–1917. https://doi.org/10.1080/19443994.2014.954148.

[10] Z. Al-Qodah, A. Al-Bsoul, E. Assirey, M. Al-Shannag, Combined ultrasonic irradiation and aerobic biodegradation treatment for olive mills wastewaters, Environ. Eng. Manag. J. 13 (2014) 2109–2118. https://doi.org/10.30638/eemj.2014.233.

[11] Y. Zhu, J. Nie, X. Yang, X. Guan, Degradation of tetrabromobisphenol A by ferrate(VI)-CaSO3 process: Kinetics, products, and impacts on following disinfection by-products formation, J. Hazard. Mater. 412 (2021) 125297. https://doi.org/10.1016/j.jhazmat.2021.125297.

[12] B.G. Savić, D.M. Stanković, S.M. Živković, M.R. Ognjanović, G.S. Tasić, I.J. Mihajlović, T.P. Brdarić, Electrochemical oxidation of a complex mixture of phenolic compounds in the base media using PbO2-GNRs anodes, Appl. Surf. Sci. 529 (2020). https://doi.org/10.1016/j.apsusc.2020.147120.

[13] S. Golbaz, A.J. Jafari, M. Rafiee, R.R. Kalantary, Separate and simultaneous removal of phenol, chromium, and cyanide from aqueous solution by coagulation/precipitation: Mechanisms and theory, Chem. Eng. J. 253 (2014) 251–257. https://doi.org/10.1016/j.cej.2014.05.074.

713 [14] C.M. Sánchez-Arévalo, Á. Jimeno-Jiménez, C. Carbonell-Alcaina, M.C. Vincent-Vela, S.
714 Álvarez-Blanco, Effect of the operating conditions on a nanofiltration process to separate
715 low-molecular-weight phenolic compounds from the sugars present in olive mill
716 wastewaters, Process Saf. Environ. Prot. 148 (2021) 428–436.
717 https://doi.org/10.1016/j.psep.2020.10.002.

718 [15] J.M. Ochando-Pulido, J.A. Vellido-Pérez, R. González-Hernández, A. Martínez-Férez,
719 Optimization and modeling of two-phase olive-oil washing wastewater integral treatment
720 and phenolic compounds recovery by novel weak-base ion exchange resins, Sep. Purif.
721 Technol. 249 (2020) 117084. https://doi.org/10.1016/j.seppur.2020.117084.

722 [16] R. Sulaiman, I. Adeyemi, S.R. Abraham, S.W. Hasan, I.M. AlNashef, Liquid-liquid
723 extraction of chlorophenols from wastewater using hydrophobic ionic liquids, J. Mol. Liq.
724 294 (2019) 111680. https://doi.org/10.1016/j.molliq.2019.111680.

725 [17] B.M. Mareai, M. Fayed, S.A. Aly, W.I. Elbarki, Performance comparison of phenol
726 removal in pharmaceutical wastewater by activated sludge and extended aeration
727 augmented with activated carbon, Alexandria Eng. J. 59 (2020) 5187–5196.
728 https://doi.org/10.1016/j.aej.2020.09.048.

729 [18] A.A. Oladipo, Rapid photocatalytic treatment of high-strength olive mill wastewater by
730 sunlight and UV-induced CuCr2O4@CaFe–LDO, J. Water Process Eng. 40 (2021) 101932.
731 https://doi.org/10.1016/j.jwpe.2021.101932.

732 [19] A.A. Oladipo, CuCr2O4@CaFe–LDO photocatalyst for remarkable removal of COD from
733 high-strength olive mill wastewater, J. Colloid Interface Sci. 591 (2021) 193–202.
734 https://doi.org/10.1016/j.jcis.2021.01.080.

[20] S. Sklavos, G. Gatidou, A.S. Stasinakis, D. Haralambopoulos, Use of solar distillation for olive mill wastewater drying and recovery of polyphenolic compounds, J. Environ. Manage. 162 (2015) 46–52. https://doi.org/10.1016/j.jenvman.2015.07.034.

[21] A. Al Bsoul, M. Hailat, A. Abdelhay, M. Tawalbeh, A. Al-Othman, I.N. Al-kharabsheh, A.A. Al-Taani, Efficient removal of phenol compounds from water environment using Ziziphus leaves adsorbent, Sci. Total Environ. 761 (2021) 143229. https://doi.org/10.1016/j.scitotenv.2020.143229.

[22] S. Senel, A. Kara, G. Alsancak , A. Denizli, Removal of phenol and chlorophenols from water with reusable dye-affinity hollow fibers, 138 (2006) 317–324. https://doi.org/10.1016/j.jhazmat.2006.05.121.

[23] B. Osman, E. T. Ozer, A. Kara, E. Yesilova, N. Besirli, Properties of magnetic microbeads in removing bisphenol-A from aqueous phase, (2015) 37–46. https://doi.org/10.1007/s10934-014-9870-z.

[24] A. Supong, P.C. Bhomick, R. Karmaker, S.L. Ezung, L. Jamir, U.B. Sinha, D. Sinha, Experimental and theoretical insight into the adsorption of phenol and 2,4-dinitrophenol onto Tithonia diversifolia activated carbon, Appl. Surf. Sci. 529 (2020) 147046. https://doi.org/10.1016/j.apsusc.2020.147046.

[25] J. Heydaripour, M. Gazi, A.A. Oladipo, H.O. Gulcan, A novel magnetic mesoporous resorcinol–melamine–formaldehyde resin for removal of phenols from aqueous solution, J. Porous Mater. 26 (2019) 1249–1258. https://doi.org/10.1007/s10934-018-0714-0.

[26] J. Heydaripour, M. Gazi, A.A. Oladipo, H.O. Gulcan, Porous magnetic resin-g-chitosan beads for adsorptive removal of phenolic compounds, Int. J. Biol. Macromol. 123 (2019)

1125–1131. https://doi.org/10.1016/j.ijbiomac.2018.11.168.

[27] N. Baig, Ihsanullah, M. Sajid, T.A. Saleh, Graphene-based adsorbents for the removal of toxic organic pollutants: A review, J. Environ. Manage. 244 (2019) 370–382. https://doi.org/10.1016/j.jenvman.2019.05.047.

[28] A.F. de Almeida Neto, M.G.A. Vieira, M.G.C. da Silva, Adsorption and desorption processes for copper removal from water using different eluents and calcined clay as adsorbent, J. Water Process Eng. 3 (2014) 90–97. https://doi.org/10.1016/j.jwpe.2014.05.014.

[29] K. Al-Malah, M.O.J. Azzam, N.I. Abu-Lail, Olive mills effluent (OME) wastewater post-treatment using activated clay, Sep. Purif. Technol. 20 (2000) 225–234. https://doi.org/10.1016/S1383-5866(00)00114-3.

[30] S.M. Lee, Thanhmingliana, D. Tiwari, Hybrid materials precursor to natural clay in the attenuation of bisphenol A from aqueous solutions, J. Water Process Eng. 11 (2016) 46–54. https://doi.org/10.1016/j.jwpe.2016.03.007.

[31] S. Peng, T. Mao, C. Zheng, X. Wu, Y. Wei, Z. Zeng, R. Xiao, Y. Sun, Polyhydroxyl gemini surfactant-modified montmorillonite for efficient removal of methyl orange, Colloids Surfaces A Physicochem. Eng. Asp. 578 (2019). https://doi.org/10.1016/j.colsurfa.2019.123602.

[32] M. Tokarčíková, J. Seidlerová, O. Motyka, O. Životský, K. Drobíková, R. Gabor, Experimental verification of regenerable magnetically modified montmorillonite and its application for heavy metals removal from metallurgical waste leachates, J. Water Process Eng. 39 (2021). https://doi.org/10.1016/j.jwpe.2020.101691.

[33] N. Dobe, D. Abia, C. Tcheka, J.P.N. Tejeogue, M. Harouna, Removal of amaranth dye by modified Ngassa clay: Linear and non-linear equilibrium, kinetics and statistical study, Chem. Phys. Lett. 801 (2022) 139707. https://doi.org/10.1016/j.cplett.2022.139707.

[34] T. Chauhan, M. Udayakumar, M. Ahmed Shehab, F. Kristály, A. Katalin Leskó, M. Ek, D. Wahlqvist, P. Tóth, K. Hernadi, Z. Németh, Synthesis, characterization, and challenges faced during the preparation of zirconium pillared clays, Arab. J. Chem. 15 (2022). https://doi.org/10.1016/j.arabjc.2022.103706.

[35] D. Chen, C. Cen, J. Feng, C. Yao, W. Li, S. Tian, Y. Xiong, Co-catalytic effect of Al-Cr pillared montmorillonite as a new SCR catalytic support, J. Chem. Technol. Biotechnol. 91 (2016) 2842–2851. https://doi.org/10.1002/jctb.4899.

[36] A. Sampieri, G. Fetter, P. Bosch, S. Bulbulian, Washing effect on the synthesis of silica-pillared clays, J. Porous Mater. 11 (2004) 157–162. https://doi.org/10.1023/B:JOPO.0000038011.54378.9e.

[37] N. Bueno, A. Pérez, R. Molina, S. Moreno, Pillared bentonite from Al-Fe-Cu polymeric precursor in solid state for the catalytic oxidation of amoxicillin, Catal. Today. 418 (2023). https://doi.org/10.1016/j.cattod.2023.114135.

[38] M. Chauhan, V.K. Saini, S. Suthar, Ti-pillared montmorillonite clay for adsorptive removal of amoxicillin, imipramine, diclofenac-sodium, and paracetamol from water, J. Hazard. Mater. 399 (2020) 122832. https://doi.org/10.1016/j.jhazmat.2020.122832.

[39] Y. Cardona, S.A. Korili, A. Gil, A nonconventional aluminum source in the production of alumina-pillared clays for the removal of organic pollutants by adsorption, Chem. Eng. J. 425 (2021) 130708. https://doi.org/10.1016/j.cej.2021.130708.

[40] X. yun Zou, F. Xiao, S. rong Liu, X. qiang Cao, L. Li, M. Chen, L. Dong, X. jun Lyu, Y. jie Gai, Preparation and application of CPC/Keggin-Al30 modified montmorillonite composite for Cr (VI) removal, J. Water Process Eng. 37 (2020) 101348. https://doi.org/10.1016/j.jwpe.2020.101348.

[41] M.E. Roca Jalil, R.S. Vieira, D. Azevedo, M. Baschini, K. Sapag, Improvement in the adsorption of thiabendazole by using aluminum pillared clays, Appl. Clay Sci. 71 (2013) 55–63. https://doi.org/10.1016/j.clay.2012.11.005.

[42] A.M. Garcia-Mora, R.A. Torres-Palma, H. García, A. Hidalgo-Troya, L.A. Galeano, Removal of dissolved natural organic matter by the Al/Fe pillared clay-activated-catalytic wet peroxide oxidation: Statistical multi-response optimization, J. Water Process Eng. 39 (2021). https://doi.org/10.1016/j.jwpe.2020.101755.

[43] Y. Cardona, A. Węgrzyn, P. Miśkowiec, S.A. Korili, A. Gil, Heterogeneous Fenton- and photo-Fenton-like catalytic degradation of emerging pollutants using Fe2O3/TiO2/pillared clays synthesized from aluminum industrial wastes, J. Water Process Eng. 52 (2023). https://doi.org/10.1016/j.jwpe.2023.103494.

[44] J.H. Hasperué, L.M. Rodoni, L.M. Guardianelli, A.R. Chaves, G.A. Martínez, Use of LED light for Brussels sprouts postharvest conservation, Sci. Hortic. (Amsterdam). 213 (2016) 281–286. https://doi.org/10.1016/j.scienta.2016.11.004.

[45] J. Zhu, K. Wen, P. Zhang, Y. Wang, L. Ma, Y. Xi, R. Zhu, H. Liu, H. He, Keggin-Al30 pillared montmorillonite, Microporous Mesoporous Mater. 242 (2017) 256–263. https://doi.org/10.1016/j.micromeso.2017.01.039.

[46] M. Altunlu, S. Yapar, Effect of OH-/Al3+ and Al3+/clay ratios on the adsorption properties

of Al-pillared bentonites, Colloids Surfaces A Physicochem. Eng. Asp. 306 (2007) 88–94. https://doi.org/10.1016/j.colsurfa.2006.10.071.

[47] H. Desai, K. A, G.S.K. Reddy, Sustainable and rapid pillared clay synthesis with applications in removal of anionic and cationic dyes, Microporous Mesoporous Mater. 352 (2023) 112488. https://doi.org/10.1016/j.micromeso.2023.112488.

[48] S. Zuo, R. Zhou, C. Qi, Synthesis and characterization of aluminum and Al/REE pillared clays and supported palladium catalysts for benzene oxidation, J. Rare Earths. 29 (2011) 52–57. https://doi.org/10.1016/S1002-0721(10)60393-6.

[49] M.A. De León, C. De Los Santos, L. Latrónica, A.M. Cesio, C. Volzone, J. Castiglioni, M. Sergio, High catalytic activity at low temperature in oxidative dehydrogenation of propane with Cr-Al pillared clay, Chem. Eng. J. 241 (2014) 336–343. https://doi.org/10.1016/j.cej.2013.10.086.

[50] E. Bazrafshan, F.K. Mostafapour, A.H. Mahvi, Phenol removal from aqueous solutions using pistachio-nut shell ash as a low cost adsorbent, Fresenius Environ. Bull. 21 (2012) 2962–2968.

[51] M. Ahmadi, M. Hazrati Niari, B. Kakavandi, Development of maghemite nanoparticles supported on cross-linked chitosan (γ-Fe2O3@CS) as a recoverable mesoporous magnetic composite for effective heavy metals removal, J. Mol. Liq. 248 (2017) 184–196. https://doi.org/10.1016/j.molliq.2017.10.014.

[52] Y. Dehmani, L. Sellaoui, Y. Alghamdi, J. Lainé, M. Badawi, A. Amhoud, A. Bonilla-Petriciolet, T. Lamhasni, S. Abouarnadasse, Kinetic, thermodynamic and mechanism study of the adsorption of phenol on Moroccan clay, J. Mol. Liq. 312 (2020).

https://doi.org/10.1016/j.molliq.2020.113383.

[53] H. Wang, D. Zhang, Y. Zhao, M. Xie, Cationic surfactant modified attapulgite for removal of phenol from wastewater, Colloids Surfaces A Physicochem. Eng. Asp. 641 (2022) 128479. https://doi.org/10.1016/j.colsurfa.2022.128479.

[54] Y. Dehmani, O. El Khalki, H. Mezougane, S. Abouarnadasse, Comparative study on adsorption of cationic dyes and phenol by natural clays, Chem. Data Collect. 33 (2021) 100674. https://doi.org/10.1016/j.cdc.2021.100674.

[55] I.A.W. Tan, A.L. Ahmad, B.H. Hameed, Adsorption isotherms, kinetics, thermodynamics and desorption studies of 2,4,6-trichlorophenol on oil palm empty fruit bunch-based activated carbon, J. Hazard. Mater. 164 (2009) 473–482. https://doi.org/10.1016/j.jhazmat.2008.08.025.

[56] M. Aazza, H. Ahlafi, H. Moussout, H. Maghat, Adsorption of metha-nitrophenol onto alumina and HDTMA modified alumina: Kinetic, isotherm and mechanism investigations, J. Mol. Liq. 268 (2018) 587–597. https://doi.org/10.1016/j.molliq.2018.07.095.

[57] A. El Gaidoumi, A. Chaouni Benabdallah, A. Lahrichi, A. Kherbeche, Adsorption du phénol en milieu aqueux par une pyrophyllite marocaine brute et traitée, J. Mater. Environ. Sci. 6 (2015) 2247–2259.

[58] M.A. Adebayo, F.I. Areo, Removal of phenol and 4-nitrophenol from wastewater using a composite prepared from clay and Cocos nucifera shell: Kinetic, equilibrium and thermodynamic studies, Resour. Environ. Sustain. 3 (2021) 100020. https://doi.org/10.1016/j.resenv.2021.100020.

[59] J.B. Rial, M.L. Ferreira, Potential applications of spent adsorbents and catalysts: Re-

867 valorization of waste, Sci. Total Environ. 823 (2022).
868 https://doi.org/10.1016/j.scitotenv.2022.153370.

869

870

871 Figure 1

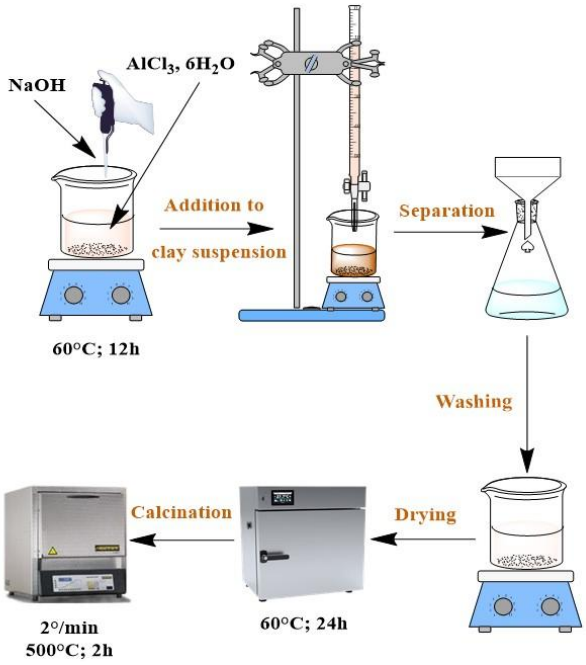

872

873

874 Figure 2

875

876

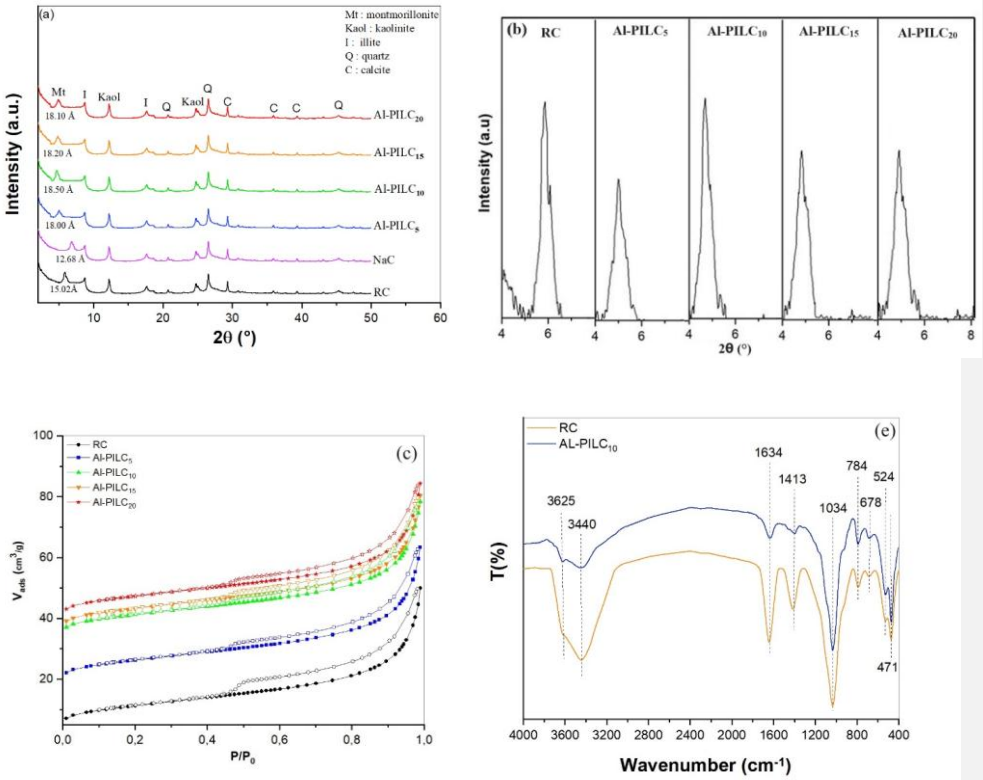

877 Figure 3

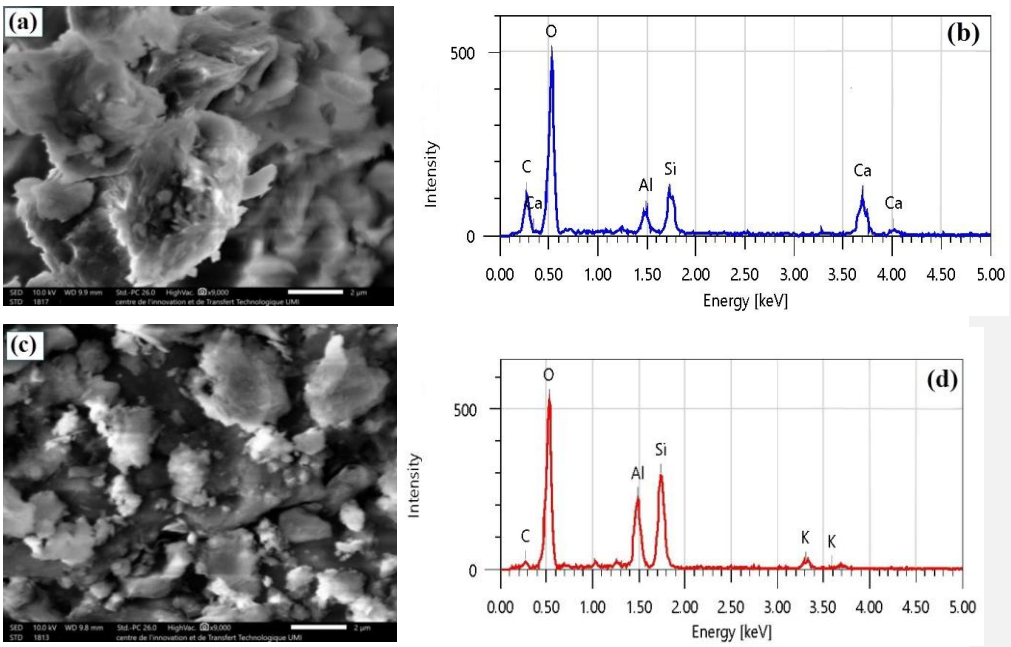

878

879 Figure 4

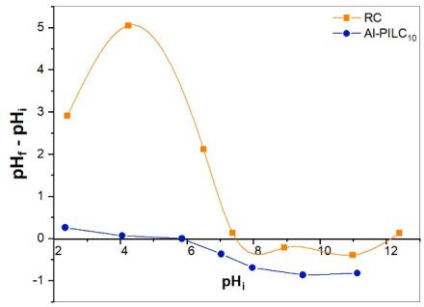

880

881 Figure 5

882

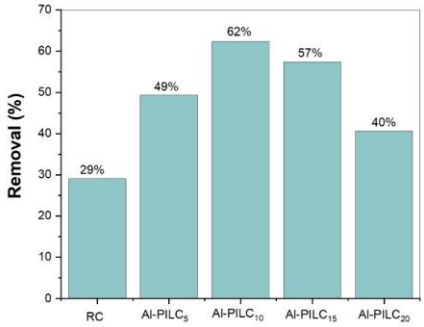

883

884

885

886 Figure 6

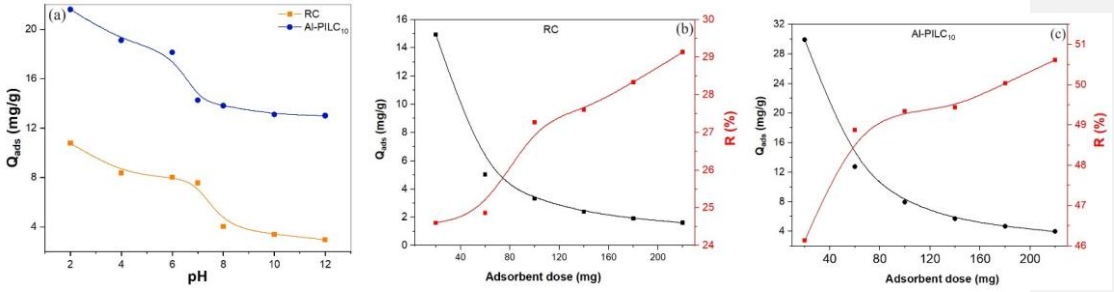

887

888 Figure 7

889

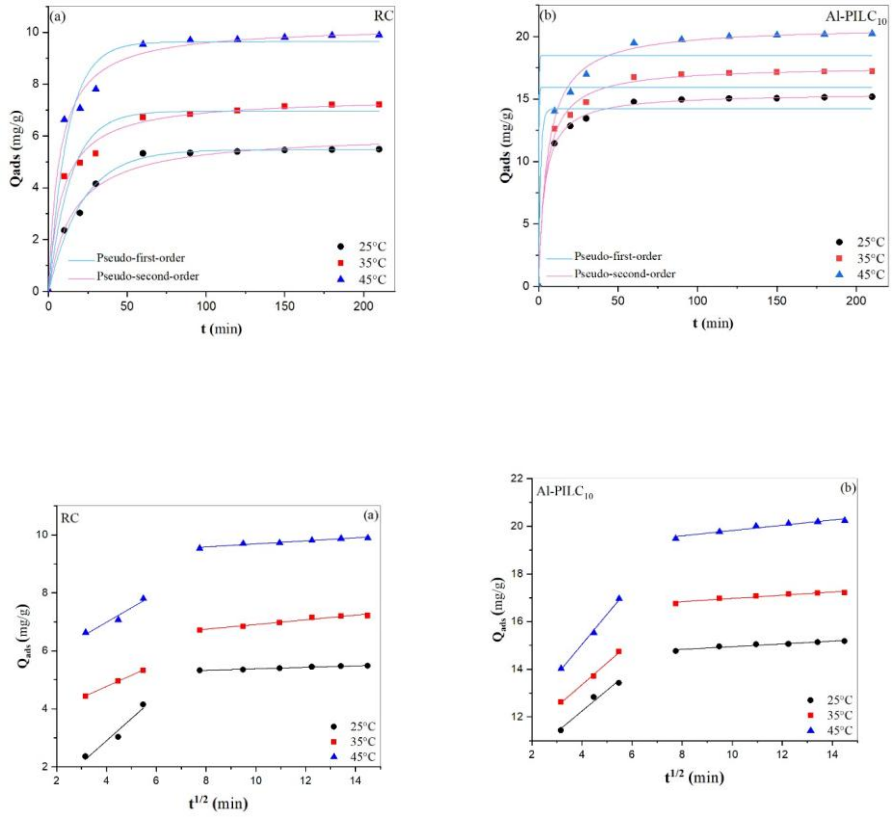

890 Figure 8

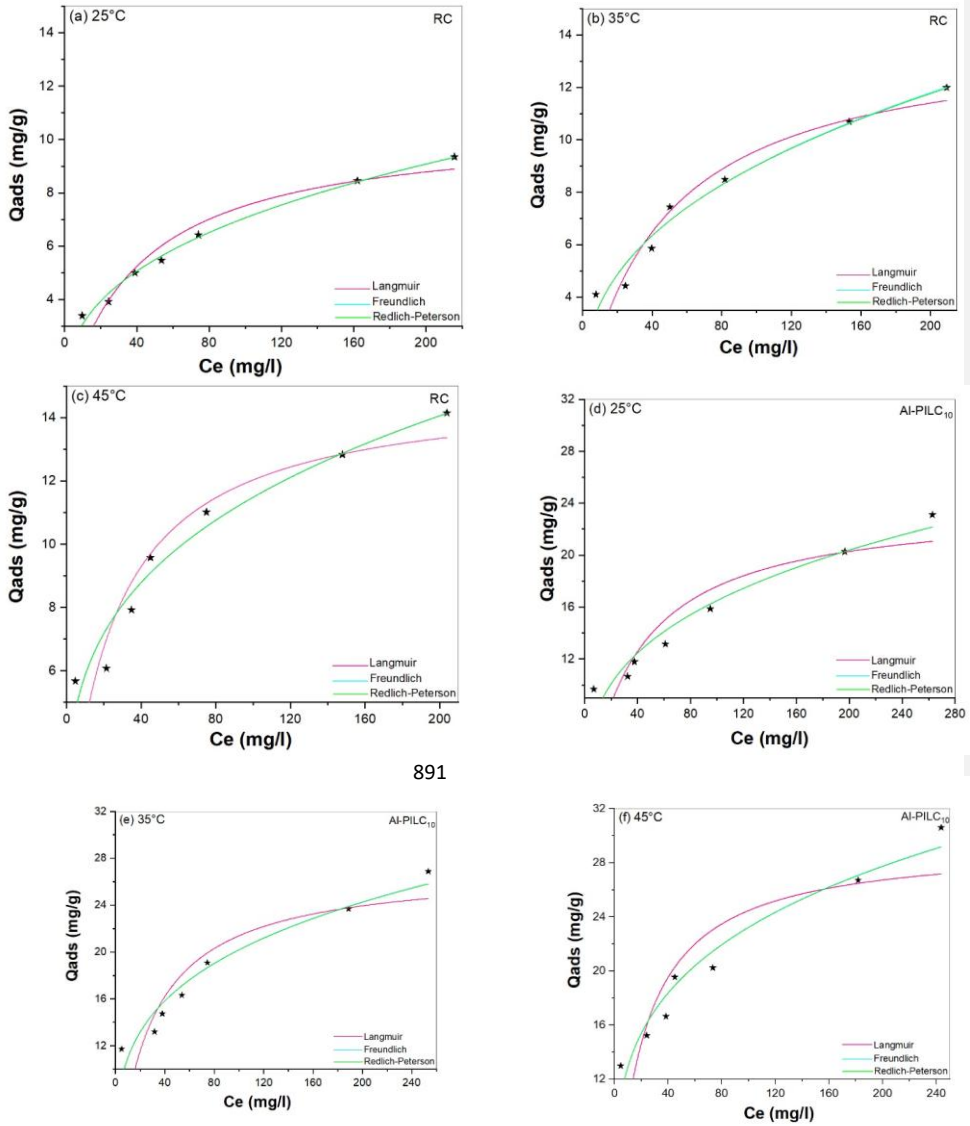

891

892

893

894

895

896 Figure 9

897

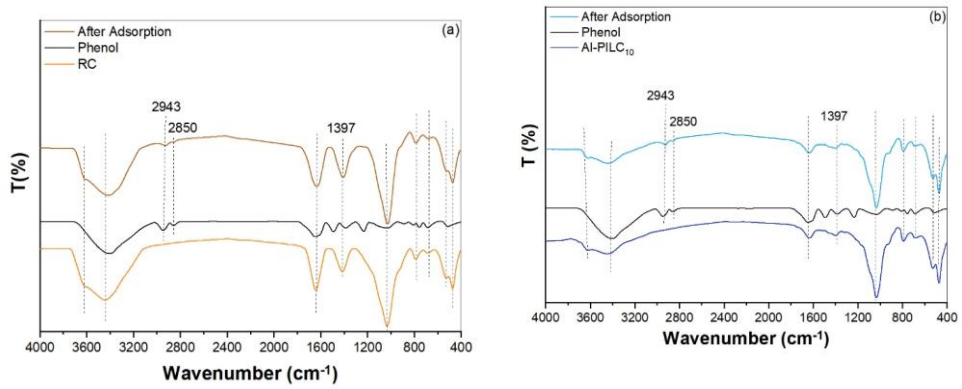

899 Figure 10

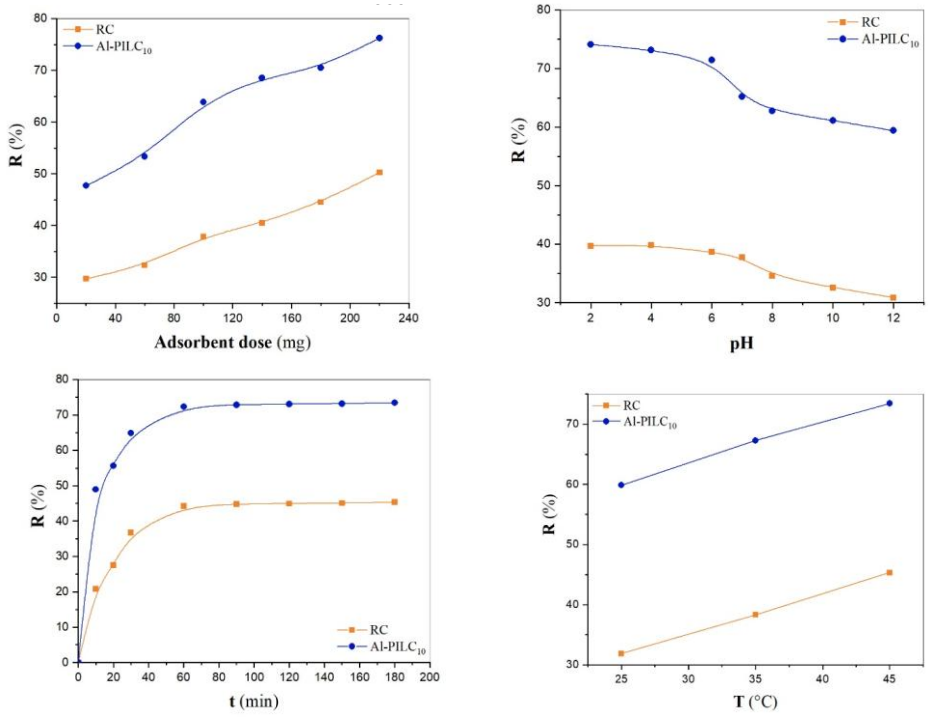

Figure 11

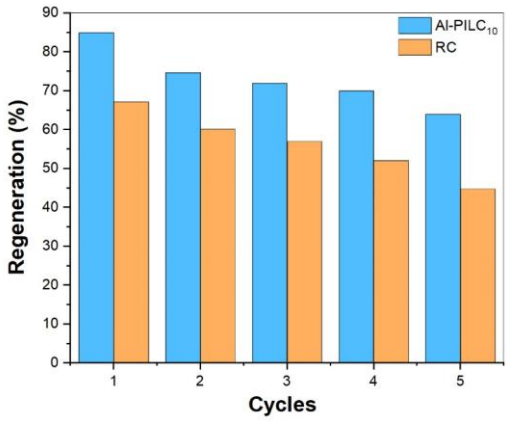

Figure 12

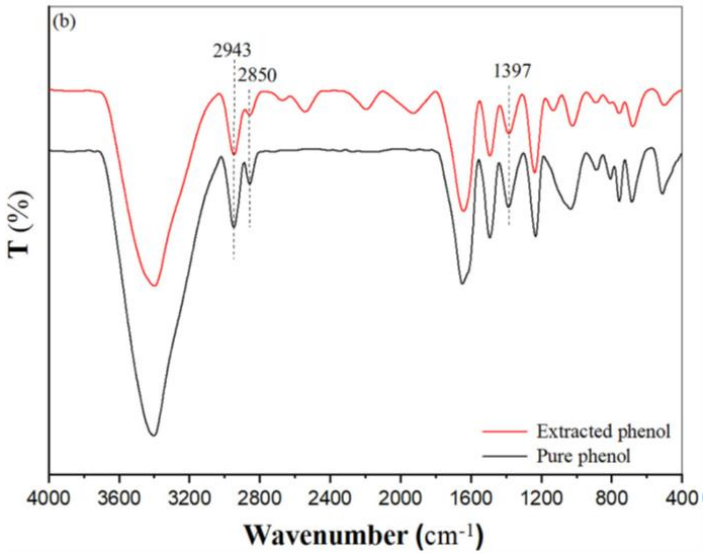

916 Table 1. Kinetic and isothermal models.

	Kinetic models	Ref
Pseudo first order	$q_t = q_e\left(1\_e^{-k_1 t}\right)$	[32]
Pseudo second order	$q_t = \frac{q_e^2 k_2 t}{q_e k_2 t + 1}$	[32]
Weber and Morris	$q_t = k_{id}\sqrt{t} + C_i$	[17]
	Isotherms models	
Langmuir	$q_e = \frac{q_m K_L C_e}{1+K_L C_e}$	[17]
Freundlich	$q_e = K_F C_e^{1/n}$	[17]
Redlich-Peterson	$q_e = \frac{AC_e}{1+K_R(C_e)^{\beta}}$	[47]
	$A = K_R q_m$	
	Error functions	
Standard deviation : Δq (%)	$\Delta q(\%) = 100 \times \left\{\frac{\sum_{i=1}^{n}\left[\left(q_{exp}-q_{cal}\right)/q_{exp}\right]^2}{n-1}\right\}^{1/2}$	[32]
Chi-square : χ^2	$\chi^2 = \sum_{i=1}^{n}\frac{(q_{exp}-q_{cal})^2}{q_{cal}}$	[15]
Coefficient of determination : R^2	$R^2 = \frac{\sum_{i=1}^{n}(q_{cal}-q_{exp})^2}{\sum_{i=1}^{n}(q_{cal}-q_{exp})^2 + \sum_{i=1}^{n}(q_{cal}-q_{exp})^2}$	[32]

917

918 Where q_e: adsorption capacity at equilibrium (mg/g), q_t: adsorption capacity at time t (mg/g), k_1: pseudo-
919 first-order rate constant (1/min), k_2: pseudo-second-order rate constant (g/mg.min), k_{id}: intra-particle
920 diffusion rate constant ($min^{1/2}$.mg/g), C: thickness of the boundary layer, C_e is the equilibrium concentration
921 (mol/L), q_m is the maximum amount adsorbed for formation of a complete monolayer on the surface of the
922 adsorbent (mg of pollutant/g of adsorbent), K_F and n are Freundlich constants that express the capacity and
923 the adsorption intensity, respectively and K_R and β ($0 < \beta < 1$) are the R-P constants.

924 Table 2. Micropore structure parameters of RC and synthesized Al-PILCs.

Samples	BET Surface Area (m^2/g)	Total Pore Volume (cm^3/g)	Micropore Volume (cm^3/g)	Average Pore Diameter (Å)
RC	40	0.0583	0.0174	57.96
Al-PILC$_5$	97	0.1084	0.0406	49.97
Al-PILC$_{10}$	127	0.1383	0.0639	37.62
Al-PILC$_{15}$	132	0.1465	0.0670	33.51
Al-PILC$_{20}$	141	0.1592	0.0732	24.62

925

926 Table 3. Chemical composition of RC and Al-PILC$_{10}$.

Adsorbent	SiO_2	Al_2O_3	CaO	Fe_2O_3	K_2O	MgO	MnO	Na_2O	P_2O_5	TiO_2	LOI
RC	42.46	14.25	12.12	6.34	2.14	3.08	0.05	<0.01	0.21	0.71	18.64
Al-PILC$_{10}$	42.97	18.05	11.30	7.01	2.32	3.04	0.05	<0.02	0.23	0.72	14.69

927

928 LOI is the Loss-on-ignition at 950 °C

929

930

931

932

933

934

935

936

Table 4. Kinetic parameters of Phenol adsorption at different temperatures onto RC and Al-PILC$_{10}$.

	Sample	RC			Al-PILC		
	T (°C)	25	35	45	25	35	45
Pseudo first order	k_1(1/min)	0.047	0.071	0.082	0.762	3.851	4.215
	q_{e1} (mg/g)	4.466	6.956	8.628	14.20	15.934	18.480
	R_1^2	0.992	0.961	0.962	0.927	0.900	0.873
	X^2	0.028	0.218	0.400	1.780	3.147	5.569
	Δq (%)	0.074	0.193	0.256	0.471	0.591	0.786
Pseudo second order	k_2 (g/mg.min)	0.010	0.015	0.014	0.017	0.012	0.008
	q_{e2} (mg/g)	5.898	7.487	10.025	15.46	17.64	20.82
	R_2^2	0.984	0.988	0.987	0.998	0.995	0.995
	X^2	0.063	0.064	0.132	0.028	0.148	0.199
	Δq (%)	0.173	0.147	0.200	0.085	0.198	0.237

946 Table 6. Model parameters for phenol adsorption on RC and Al-PILC$_{10}$ at different temperatures.

		RC			Al-PILC$_{10}$		
Model	**Parameters**	**25°C**	**35°C**	**45°C**	**25°C**	**35°C**	**45°C**
Langmuir	**q_m (mg/g)**	10.55	14.07	14.97	23.94	27.181	29.429
	K_L (L/mg)	0.024	0.021	0.041	0.027	0.036	0.049
	R^2	0.915	0.900	0.799	0.711	0.638	0.650
	χ^2	0.505	1.090	2.565	8.957	13.60	16.80
Freundlich	**K_F (mg/g)**	1.325	1.526	2.995	4.031	5.959	7.147
	1/n	0.363	0.384	0.291	0.305	0.265	0.256
	R^2	0.991	0.968	0.950	0.941	0.935	0.946
	χ^2	0.052	0.348	0.635	1.830	2.438	2.589
Redlich-Peterson	**K_{RP}**	9.4^E3	9.8^E2	2.9^E8	6.7^E4	3.4^E4	3.2^E4
	A	1.2^E4	1.5^E3	8.9^E8	2.7^E5	2.0^E5	2.3^E5
	ß	0.636	0.616	0.708	0.694	0.735	0.744
	R^2	0.991	0.968	0.950	0.941	0.935	0.946
	χ^2	0.066	0.435	0.794	2.287	3.048	3.236

947

948

Table 7. Thermodynamic parameters of phenol adsorption by RC and Al-PILC$_{10}$.

	T (°C)	ΔH° (kJ.mol)	ΔS° (kJ/K.mol)	ΔG° (kJ/mol)
RC	25	31.88	0.108	-0.304
	35			-1.384
	45			-2.464
Al-PILC$_{10}$	25	22.64	0.087	-3.306
	35			-4.176
	45			-5.046

Table 8. OMW characterization before and after treatment using RC and Al-PILC$_{10}$.

Parameters	**Before treatment**	**After treatment**	
		RC	**Al-PILC$_{10}$**
pH	4.52	5.89	6.32
Conductivity (mSC^{-1})	16.22	14.03	11.92
Turbidity (NTU)	1930	1154	694
BOD$_5$ (g of O$_2$/l)	17.23	12.10	7.73
COD (g of O$_2$/l)	84.10	66.25	49.13
Phenolic compounds (mg/L)	334.72	166.84	80.30